Transactions of The Indian Institute of Metals
Vol. 64, Issues 1 & 2, February-April 2011, pp. 57-61

Study of Brittle-to-ductile-transition in Pt-aluminide bond coat using micro-tensile testing method

Md Zafir Alam[1], B. Srivathsa[1], S.V. Kamat[1], V. Jayaram[2] and D.K. Das[1]

[1] *Defence Metallurgical Research Laboratory, Hyderabad 500 058, India*
[2] *Indian Institute of Science, Bangalore 560 012, India*

E-mail : zafir@dmrl.drdo.in

Received 03 November 2010
Revised 26 January 2011
Accepted 04 February 2011
Online at www.springerlink.com

Keywords:
brittle-ductile-transition-temperature (BDTT); Pt-aluminide coatings; micro-tensile testing; dislocation climb

Abstract

The Brittle-to-ductile-transition-temperature (BDTT) of free-standing Pt-aluminide (PtAl) coating specimens, i.e. stand-alone coating specimens without any substrate, was determined by micro-tensile testing technique. The effect of Pt content, expressed in terms of the thickness of initial electro-deposited Pt layer, on the BDTT of the coating has been evaluated and an empirical correlation drawn. Increase in the electro-deposited Pt layer thickness from nil to 10 μm was found to cause an increase in the BDTT of the coating by about 100°C.

1. Introduction

Nickel based superalloy components operating in the hot sections of advanced gas turbine engines are usually applied with a Pt-aluminide (PtAl) bond coat for enhancing their high temperature oxidation resistance [1,2]. The oxidation resistance of the coating is derived from the Al atoms present in the constituent B2-NiAl phase, which form an adherent layer of α-Al_2O_3 on the surface during thermal exposure [1,2]. Additions of Pt are known to improve the oxidation resistance of these coatings, primarily by enhancing the spallation resistance of the alumina scale [3-5], reduction in the growth stresses in the alumina scale [6,7] and promoting outward diffusion of Al to form the protective alumina layer on the surface [8-10]. It is for these beneficial effects of Pt, that the PtAl coatings typically contain about 5-15 at.% Pt.

Despite their excellent oxidation resistance, the PtAl coatings have fairly high brittle-to-ductile transition temperature (BDTT), typically above 650°C [11-15]. Therefore, these coatings are prone to cracking at low temperatures, especially under cyclic heating and cooling conditions in gas turbine engines, which can potentially degrade the overall mechanical response of the coated component [2,16]. Increased Pt content in the coatings, though on one hand can impart enhanced oxidation resistance, but it has a detrimental effect in terms of increasing the BDTT of these coatings [12]. In this context, accurate determination of BDTT of PtAl coatings becomes important with respect to their Pt content. Such studies can be also effective in optimizing the oxidation as well as tensile properties of the PtAl coatings.

Unlike the case of bulk materials, where impact tests are employed to determine the BDTT, the low thickness of a PtAl coating precludes the use of such a technique for the determination of BDTT. Therefore, alternate methods have been adopted for evaluating the BDTT of bond coats. Most of the earlier work on the BDTT determination of bond coats has been carried out using tensile testing of coated superalloy specimens at various temperatures. In these tests, the strain-to-first-crack formation was detected using acoustic emission (AE) techniques [11,12]. The temperature beyond which the coating accommodates a strain of 0.6% without cracking was defined as the BDTT [11,12]. The choice of 0.6% strain was based on certain design considerations of the superalloy component. The BDTT values for various PtAl bond coats determined by the above technique have been reported to lie in the range 850-1000ºC [11,12]. Further, it has been shown that the BDTT values for PtAl coatings are usually 150-200ºC higher than those for plain aluminide coatings, i.e. coatings without Pt [12].

However, the BDTT determined using tensile testing of a coated bulk specimen involves simultaneous deformation of both substrate and the coating. Given the vast difference in the section sizes of these two constituents in the coated tensile specimen, there is a likelihood of the substrate influencing the deformation characteristics of the coating. Therefore, the transition temperature determined by the above mentioned technique of testing the bulk coated samples may not be accurate, although the determined transition temperature can provide a qualitative indication of the BDTT of the bond coat. In recent years, determination of BDTT of PtAl bond coats by direct testing of the free-standing coating has been reported. Since the coating alone is tested in these methods, the influence of the substrate is eliminated. Therefore, the BDTT values determined by these methods are expected to be more accurate. Eskner et al. [13] have evaluated BDTT by carrying out bend tests on miniaturized disc specimens of a free-standing bond coat. In another study, Pan et al. have shown the feasibility of using microtensile testing of free-standing PtAl coatings for determining the BDTT [14].

Using the microtensile testing technique, a method based on the variation in the plastic-strain-to-fracture, was proposed for the accurate determination of BDTT of aluminide bond

coats in our recent publication [15]. In the present study, a similar approach has been adopted for evaluating the effect of Pt content on the BDTT of a PtAl coating. The novelty of the present work lies in the fact that the evaluation of tensile properties of brittle free-standing PtAl bond coat by micro-tensile testing is an experimental challenge involving complex specimen preparation and test procedures. Such studies on the evaluation of mechanical behavior of free-standing brittle PtAl bond coats by micro-tensile testing method are extremely limited in open literature.

2. Experimental details

2.1 Design of microsamples

Unlike tensile testing of bulk samples, for which standards for the design of tensile specimens are available, no standards exist for the design of micro-specimens. Therefore, 2D-linear elastic finite element method (LE-FEM) based simulation studies, using ANSYS 11.0, were carried out for establishing the design of micro-tensile test specimens. Appropriate boundary conditions simulating the gripping technique adopted during the experiments as shown in the schematic in Fig. 1, i.e. where-in the sample was arrested at the holding edges within slotted grips, were imposed. The effect of specimen design parameters such as holding length 'HL', fillet radius 'R', gage length 'GL', gage width 'GW' and grip head length 'GHL' on the location of stress maxima during the tensile test was ascertained. Since a tensile specimen fails at the region of maximum stress during testing, the predicted location of stress maxima determined from the simulation studies gave a direct indication of the probable location of failure of the specimens during the tensile test. The simulation studies predicted that in order to achieve a valid tensile test, i.e. to attain a stress maxima within the gage length and cause failure of the specimens within the gage length, the following correlations must be maintained amongst the dimensional parameters:- HL:R = 2:1, GL>R, GW=R and GHL>4R (see Fig. 3(a)) [17]. For all other combinations of dimensional parameters, simulation studies predicted the location of maximum stress close to the fillet regions i.e. the specimens were prone to failure at the fillet (Fig. 3(b)) [17]. Keeping into consideration the above mentioned dimensional correlations and certain experimental constraints, the values of HL, R, GL, GW and GHL were chosen as 1, 0.5, 2, 0.5 and 2.5 mm, respectively. The overall length of the specimen was 8 mm (Fig. 2). Specimens having the above dimensions were found to fail within the gage length on most occasions. Further details on the simulation studies carried out for the design of micro-samples used in the present study and the experimental validation of the simulation results can be obtained from our recent publication [17].

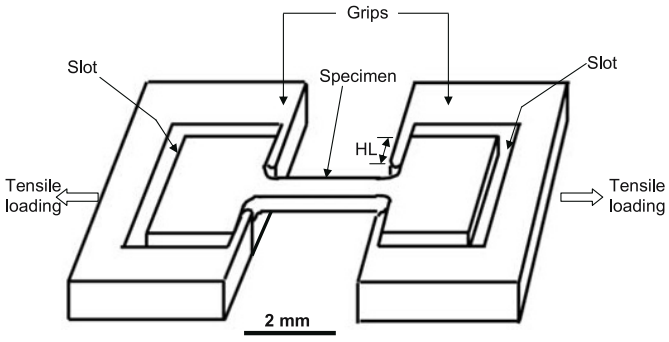

Fig. 1 : Schematic of a specimen placed within the slots present in the grips. The specimen is arrested at the holding length, HL, during tensile testing.

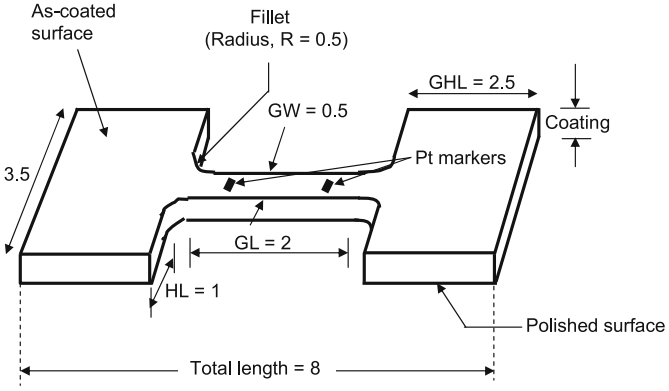

Fig. 2 : Schematic showing the sample configuration used in the present study. GL, GW, HL, R and GHL represent the gage length, gage width, holding length, fillet radius and grip head length, respectively. All dimensions are in mm.

2.2 Coating deposition

Directionally solidified Ni-based superalloy CM-247 LC was obtained in the form of cylindrical rods: 12 mm in dia. and 80 mm in length. The nominal composition of this alloy (in wt.%) is 9.2 Co-8.1 Cr-9.5 W-5.6 Al-3.2 Ta-1.5 Hf-0.7 Ti-0.015 Zr-0.5 Mo-0.15 B-0.07 C-balance Ni. About 0.5 mm thick strips were cut out from these rods by wire electro-discharge

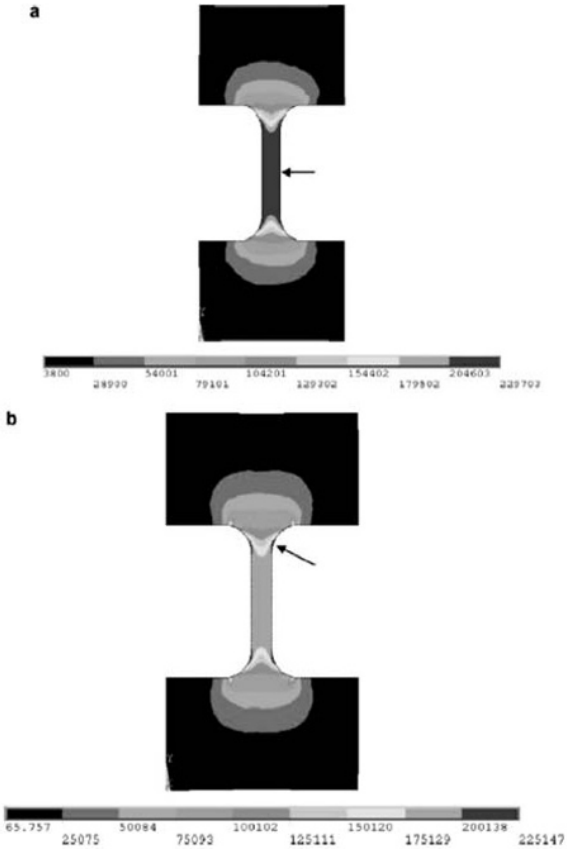

Fig. 3 : Stress contour plots for samples (a) R=GW=0.5 mm, HL=1.0 mm, GL=2.0 mm, GHL=2.5 mm and (b) R=GW=0.5 mm, HL=1.5 mm, GL=2.0 mm and GHL=2.5 mm. The location of the maximum stress has been indicated by arrows.

machining (EDM), such that the longitudinal axis of these strips was parallel to the <001> solidification direction of the rods. These strips were polished on 600 grit paper and subsequently used as substrates for coating deposition. For developing the PtAl coating, a Pt layer was electrodeposited on these strips. The Pt plated strips were then subjected to a diffusion heat treatment at 1080°C for 4 h in vacuum. Subsequently, a high activity pack aluminizing treatment, using a powder mixture of $15NiAl\text{-}3NH_4Cl\text{-}82Al_2O_3$ (compositions being in wt.%), was carried out at 850°C for 5 h in Ar atmosphere. In order to stabilize the phases formed in the coating, a post aluminizing diffusion heat treatment was carried out at 1080°C for 4 h in vacuum. PtAl coatings with varying Pt content were prepared by varying the thickness of the electro-deposited Pt layer as 0, 2, 5 and 10 μm, while other subsequent coating formation heat treatments were maintained the same as mentioned above. Henceforth, the PtAl coatings containing the initial thickness of Pt electro-deposited layer as 0, 2, 5 and 10 μm have been referred to as plain aluminide, 2PtAl, 5PtAl and 10PtAl, respectively in the text.

2.3 Micro-sample preparation

Having established the dimensions using simulation studies, micro-samples (as shown in Fig. 2), were cut out from the coated strips by means of wire EDM, as shown in Fig. 4. In order to prevent the coating from getting chipped off at the micro-sample edges, the EDM process was carried out at a low current and low feed rate. While machining of the samples, care was taken to ensure that the gage length was parallel to the longitudinal axis of the strip (Fig. 4). Subsequently, the substrate was removed by precision polishing of the micro-samples from one side until the thickness of the sample became equal to that of the coating (Fig. 2). A polishing sequence comprising 600/1500/2500 grit size polishing papers and films containing 1 and 0.5 μm size diamond particles was adopted for the above purpose. Flatness of the samples and uniformity in thickness reduction while polishing was achieved using a Tripod Polisher. The extent of thickness reduction during polishing was measured from the micrometers attached to the Tripod Polisher. Subsequently, two Pt markers were deposited on the gage length of the specimen (see Fig. 2) using a Quanta 200 3D focused ion beam (FIB) machine, operating at 20kV. These markers were used for in-situ strain measurement during testing.

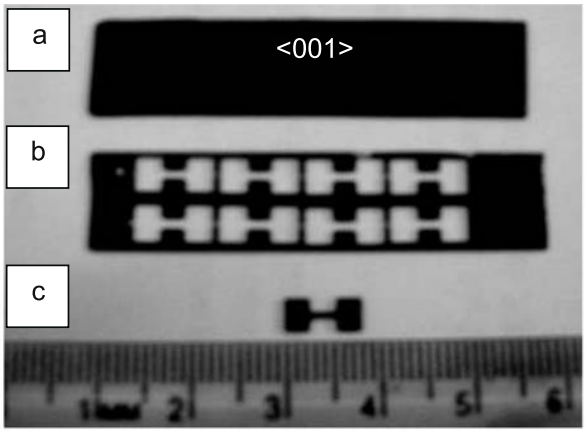

Fig. 4 : Method adopted for the fabrication of microtensile specimens: (a) PtAl coated 0.5 mm thick superalloy strip, (b) wire EDM machining of samples from the coated strip and (c) a typical cut out microtensile sample.

2.4 Testing

Tensile testing of the micro-samples was carried out at various temperatures ranging from room temperature (RT) to 950°C using a 500 N Walter-bai Ag micro-tensile testing machine. High temperature in the specimens during testing was achieved by resistance heating of the specimens by means of an impressed DC current, as proposed by Sharpe and Hemker [18]. The temperature of the specimen was monitored using a two-color ratio infra-red radiation pyrometer to an accuracy of ± 5°C. In-situ strain measurement on the samples during testing was achieved by using a non-contact video extensometer, having a resolution of 10 μ-strain. The stress-strain response of the coating was directly obtained in a computer attached to the micro-tensile testing machine. Tensile tests were carried out at an initial strain rate of 4.1×10^{-3} sec^{-1}. A constant cross head speed of 0.5 $mm.min^{-1}$ was maintained during these tests.

2.5 Microstructural observation

Microstructure and fractography studies were carried out using a Quanta 400 scanning electron microscope (SEM), operating at 20kV. A Cameca SX-100 electron probe micro-analyzer (EPMA) operating at 20 kV, was used for chemical analysis of the coating.

3. Results and discussion

3.1 Coating microstructure

The microstructure of the plain aluminide coating, shown in Fig. 5(a), exhibited a three-layer structure with an outer layer consisting of fine precipitates, an intermediate precipitate lean layer and an inner heavily precipitated inter diffusion zone (IDZ). The thickness of the above-mentioned three layers was 60, 25 and 20 μm, respectively. The matrix phase in all the three layers was constituted of the B2-NiAl phase, as determined from the XRD and the EPMA analysis. The Al concentration, was nearly constant at 45 at.% across the outer and intermediate layers. The Ni concentration in the coating was also constant at about 35 at.%.

Similar to that of the plain aluminide coating, the Pt containing coatings also exhibited a three-layer structure, as typically shown in Fig. 5(b). However, unlike the matrix phase of the plain aluminide coating which was constituted of B2-NiAl phase, the matrix phase of the Pt containing coatings was constituted of B2-(Ni,Pt)Al i.e. B2 phase containing Pt in solid solution. Further, the outer layer contained an additional $PtAl_2$ phase, as observed from the bright contrast in Fig. 5(b). The volume fraction of the $PtAl_2$ phase present in the outer layer of the coating increased from about 0.25 to 0.56 with the increase in thickness of the electrodeposited Pt layer from 2 to 10 μm. Numerous fine precipitates rich in Cr and W were present in the outer layer of the coating [19,20]. In all the PtAl coatings, the precipitate lean intermediate layer contained single phase B2-(Ni,Pt)Al and the inner layer was the heavily precipitated IDZ (Fig. 5(b)) [19,20]. The Pt content in the outer layer and the intermediate layer of the coating was found to increase from about 5-15 at.% and 1-7 at.% respectively, with the increase in thickness of the electrodeposited Pt layer from 2 to 10 μm. On the other hand, the Al and Ni concentration, however, was nearly constant at about 45 and 35 at.%, respectively, across the outer and the intermediate layers for all the PtAl coatings.

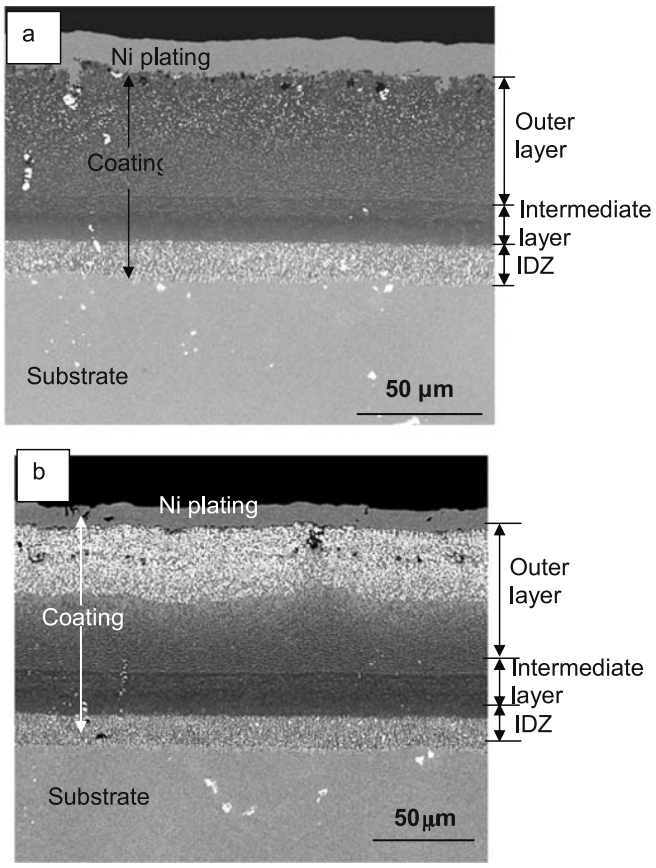

Fig. 5 : Microstructure of (a) plain aluminide (0PtAl) and (b) 5PtAl coating used in the present study.

The thickness of the various PtAl coatings was about 100 µm.

3.2 BDTT determination

The variation in the ductility, as represented by the plastic-strain-to-fracture, with test temperature for the various coatings is shown in Fig. 6. For each coating, the ductility was negligible up to a certain test temperature. Beyond this temperature, the coatings exhibited an increase in ductility. The BDTT of the coating was ascertained as the temperature corresponding to the point of intersection of the linear best fit lines drawn to the two segments of the plastic-strain-to-fracture versus temperature plots, as indicated in the inset in Fig. 6. In our recent study, the BDTT determined by such a method was found to be representative of aluminide bond coats and correlated well with the variation in the fracture surface features with test temperature, such as the presence of brittle cleavage facets below the BDTT, initiation of micro-void formation at the BDTT and formation of shallow dimples as well as fibrous fracture features above the BDTT [15]. Further, the advantages of such method of BDTT determination over other previously reported methods were also discussed [15].

3.3 Variation of BDTT with Pt content

The BDTT of the coating was found to increase with the increase in Pt content of the coating (see Fig. 6 and Table 1). While the BDTT for 0PtAl coating was 693°C, that for the 10PtAl coating was 795°C. The variation in BDTT with the Pt content of the coatings is shown in Fig. 7. Since the coating exhibits a graded microstructure and the Pt

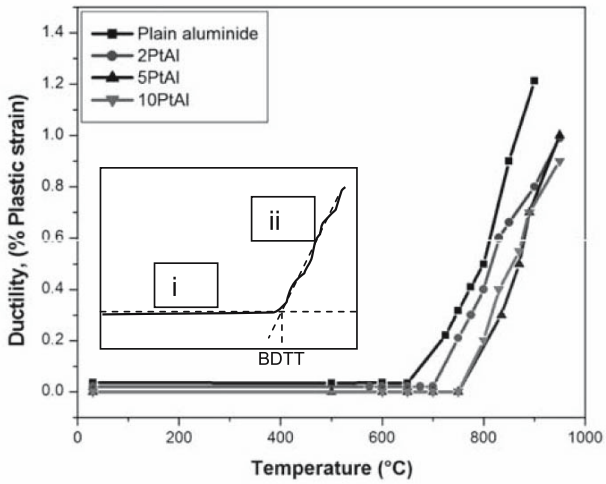

Fig. 6 : Variation of ductility (% plastic strain to fracture) with temperature for the various coatings.

concentration was non-uniform across the coating cross-section, the Pt content in the coatings has been represented in terms of the thickness of the electro-deposited Pt layer in the above figure. The variation in the BDTT with the Pt content was linear and the best-fit straight line obeyed the following equation:

$$T_{BDTT} = 698 + 10\ t_{Pt} \quad (1)$$

T_{BDTT} in the above equation stands for BDTT (°C) of the coating and t_{Pt} denotes the Pt content of the coating expressed in terms of thickness of the Pt plated layer (in µm). The correlation co-efficient, R^2, for the above linear fit was 0.98. The suitability of the above equation in correlating BDTT of the present PtAl coatings with their Pt contents was checked by evaluating the BDTT of a 7PtAl coating, i.e. the coating was prepared using a 7 µm thick Pt plated layer. The BDTT for the 7PtAl coating was found to be 775ºC, which agreed well with the predicted value of 768ºC from eq. (1).

Table 1 : BDTT of various coatings.

Sl. No.	*Coating type*	*BDTT (°C)*
1	Plain Aluminide	693
2	2PtAl	721
3	5PtAl	752
4	10PtAl	795

The inherent brittleness in the B2-NiAl phase is caused by the limited number of slip systems available for deformation, which leads to the non-fulfillment of von Mises criterion i.e. the operation of minimum five slip systems for ductility in polycrystalline materials. However, at the BDTT, the generation of additional slip systems provided by the glide and climb of <100> dislocations has been cited as a mechanism for the onset of ductile behavior in the bulk B2 phase [21,22]. In one of our recent studies, transmission electron microscopy (TEM) analysis of the dislocation behavior in free-standing PtAl coating specimens after tensile testing at the BDTT, revealed a similar mechanism involving glide and climb of <100> dislocations to be responsible for the onset of ductility in the coating [23]. It has been reported that the BDTT in bulk B2-NiAl phase is significantly affected by alloying additions such as Zr and Re [24]. Hindrance to

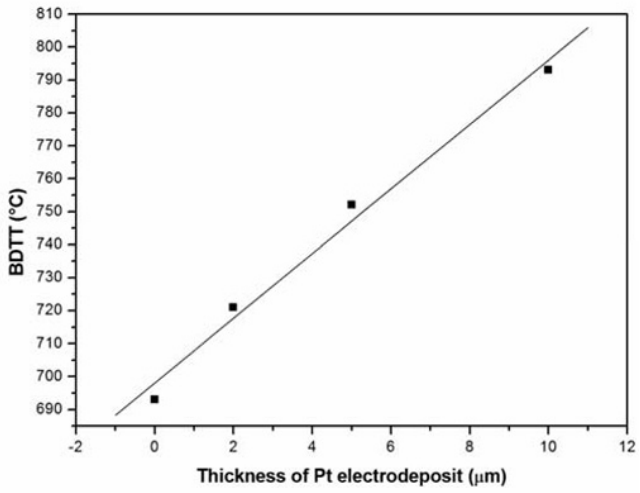

Fig. 7 : Variation of BDTT with thickness of the electrodeposited Pt layer.

dislocation glide caused by solute drag effects [25] and resistance to climb imposed by the pinning of dislocations by the solute atoms can be potential reasons causing increase in the BDTT of bulk B2-NiAl with alloying addition [24]. Based on the reasoning mentioned above, increase in the extent of alloying addition can therefore be expected to cause an increase in the BDTT. As mentioned previously, the amount of Pt present in solid solution in the B2-NiAl matrix phase of the coatings examined in the present study, increased with the increase in Pt content. Drawing analogy with the reasons stated above, the increase in the BDTT of the PtAl coating with Pt incorporation can therefore be attributed to a greater extent of hindrance to glide as well as climb of dislocations posed by the Pt atoms. The formation of an additional $PtAl_2$ phase in the outer layer of the coating (Fig. 5(b)) and increase in its volume fraction with increasing addition of Pt can also contribute to the increase in the BDTT of the coating. Presently, further studies on these aspects are being carried out and will be reported in subsequent publications.

4. Summary

The effect of Pt content on the BDTT of a free-standing PtAl bond coat has been studied. Micro-tensile testing of free-standing coating specimens was used for the above purpose. The BDTT of the coating was found to increase with the increase in Pt content of the coating.

Acknowledgements

The authors wish to acknowledge the assistance provided by the ETC, SMG, MWG and SFAG divisions of DMRL. They thank Director, DMRL, for his permission to publish this research work. This research work has been funded by the Defence Research and Development Organization (DRDO).

References

1. Pichoir R, Holmes D R and Rahmel A. (Eds.), M*aterials and Coatings to Resist High Temperature Corrosion*, Applied Science Publishers, London, (1978) 271.
2. Sudhangshu Bose, *High Temperature Coatings*, Butterworth-Heinemann Publishers, Oxford, (2007) 71.
3. Felten E J and Petit F S, *Oxid. Met.* **10** (1976) 189.
4. Felten E J, Oxid. Met. **10** (1976) 23.
5. de Wit J H W and van Manen P A, *Mater. Sci. Forum,* **154** (1994) 109.
6. Newcomb S B and Stobbs W M, Proc. Conf. on 'Elevated Temperature Coatings: Science and Technology II', Anaheim, California, USA, Warrendale, PA, *Minerals, Metals and Materials Society,* (1996) 265.
7. Allam L M, Akuezue H C and Whittle D P, *Oxid. Met.* **14** (1980) 517.
8. Tatlock G J and Hurd T J, *Oxid. Met.* **22** (1984) 201.
9. Krishna G R, Das D K, Singh V and Joshi S V, *Mater. Sci. Eng., A* **A251** (1998) 40.
10. Johnston G R, Cocking J L and Johnson W C, *Oxid. Met.* **23** (1985) 237.
11. Lowrie R and Boone D H, *Thin Solid Films,* **45** (1977) 491-498.
12. Vogel D, Newman L, Deb P and Boone D H, *Mater. Sci. Eng.* **88** (1987) 227-231.
13. Eskner M and Sandstrom R, *Surf. Coat. Technol.* **165** (2003) 71-80.
14. Pan D, Chen M W, Wright P K and Hemker K J, *Acta Mater.* **51** (2003) 2205-2217.
15. Alam M Z, Chatterjee D, Jayaram V, Kamat S V and Das D K, *Mater Sci Eng A,* **527** (2010) 7147.
16. Strang A and Lang E. Effect of Coatings on the Mechanical Properties of Superalloys, in: R. Brunetand (Eds.). In: High Temperature Alloys for Gas Turbines, D. Reidel Publishing Company, Holland; (1982) 469-506.
17. Alam M Z, Srivathsa B, Kamat S V, Jayaram V and Das D K, *Mat. Des*. (*in press*).
18. Hemker K J and Sharpe W N Jr. *Annu Rev Mater Res,* **37** (2007) 93.
19. Das D K, Vakil Singh and Joshi S V. *Metall Mater Trans A,* **31A** (2000) 2037.
20. Das D K, Vakil Singh and Joshi S V, *Metall Mater Trans A,* **29A** (1998) 2173.
21. Noebe R D, Bowman R R and Nathal M V. *Int Mater Rev*, **38**(4) (1993) 193.
22. Groves G W and Kelly A, *Phil. Mag.,* **18** (1969), 977.
23. Alam M Z, Chatterjee D, Muraleedharan K, Jayaram V, Kamat S V and Das D K, *Met Trans A* (*accepted, in press*).
24. Noebe R D, Cullers C L and Bowman R R, *J. Mater Res,* **7**(3) (1992) 605.
25. Rickman J M, LeSar R and Srolovitz D J, *Acta Mater,* **51** (2003) 1199.